Acta Pharmaceutica Sinica B 2025;15(11):5854−5866

Chinese Pharmaceutical Association
Institute of Materia Medica, Chinese Academy of Medical Sciences

Acta Pharmaceutica Sinica B

www.elsevier.com/locate/apsb
www.sciencedirect.com

ORIGINAL ARTICLE

A promising novel local anesthetic for effective anesthesia in oral inflammatory conditions through reducing mitochondria-related apoptosis

Haofan Wang[a,†], Yihang Hao[a,†], Wenrui Gai[c,†], Shilong Hu[c], Wencheng Liu[b,c], Bo Ma[a], Rongjia Shi[a], Yongzhen Tan[a], Ting Kang[c], Ao Hai[c], Yi Zhao[c], Yaling Tang[a], Ling Ye[a], Jin Liu[c], Xinhua Liang[a,*], Bowen Ke[c,*]

[a]*State Key Laboratory of Oral Diseases and National Clinical Research Center for Oral Diseases, West China Hospital of Stomatology, Sichuan University, Chengdu 610041, China*
[b]*College of Computer Science, Sichuan University, Chengdu 610065, China*
[c]*Department of Anesthesiology, Laboratory of Anesthesia and Critical Care Medicine, National-Local Joint Engineering Research Centre of Translational Medicine of Anesthesiology, Frontiers Science Center for Disease-Related Molecular Network, West China Hospital, Sichuan University, Chengdu 610041, China*

Received 24 October 2024; received in revised form 24 February 2025; accepted 30 March 2025

KEY WORDS

Oral local anesthetics;
Articaine;
Mitochondria;
Inflammatory;
Apoptosis;
Mitochondrial reactive oxygen species;
NRF2;
Sodium

Abstract Local anesthetics (LAs), such as articaine (AT), exhibit limited efficacy in inflammatory environments, which constitutes a significant limitation in their clinical application within oral medicine. In our prior research, we developed AT-17, which demonstrated effective properties in chronic inflammatory conditions and appears to function as a novel oral LA that could address this challenge. In the present study, we further elucidated the beneficial effects of AT-17 in acute inflammation, particularly in oral acute inflammation, where mitochondrial-related apoptosis played a crucial role. Our findings indicated that AT-17 effectively inhibited lipopolysaccharide (LPS)-induced nerve cell apoptosis by ameliorating mitochondrial dysfunction *in vitro*. This process involved the inhibition of mitochondrial reactive oxygen species (mtROS) production and the subsequent activation of the NRF2 pathway. Most notably, improvements in mitochondria-related apoptosis were key contributors to AT-17's inhibition of voltage-gated

*Corresponding authors.
E-mail addresses: lxh88866@scu.edu.cn (Xinhua Liang), bowenke@scu.edu.cn (Bowen Ke).
[†]These authors made equal contributions to this work.
Peer review under the responsibility of Chinese Pharmaceutical Association and Institute of Materia Medica, Chinese Academy of Medical Sciences.

https://doi.org/10.1016/j.apsb.2025.09.001

sodium channels. Additionally, AT-17 was shown to reduce mtROS production in nerve cells through the Na^+/NCLX/ETC signaling axis. In conclusion, we have developed a novel local anesthetic that exhibits pronounced anesthetic functionality under inflammatory conditions by enhancing mitochondria-related apoptosis. This advancement holds considerable promise for future drug development and deepening our understanding of the underlying mechanisms of action.

1. Introduction

It has been demonstrated that the analgesic efficacy of local anesthetics (LAs) is often inadequate in inflammatory states affecting the oral and maxillofacial regions. Consequently, patients suffering from such inflammatory conditions frequently endure significant pain both during and following surgical procedures. For instance, during the management of acute pulpitis and mandibular wisdom teeth associated with acute pericoronitis, several patients continue to experience pain even after administration of articaine (AT) anesthesia; this discomfort may persist for 4 to 6 h, or in some instances, extend up to 48 h, necessitating further analgesia or even morphine application[1,2]. Thus, there exists a critical need for the development of novel local anesthetics capable of providing effective analgesia in environments characterized by oral inflammation, which holds considerable clinical significance.

Previous research has suggested that inflammatory stimulation can induce apoptosis of nerve cells; therefore, reducing nerve cell apoptosis may be a promising approach to alleviate inflammatory pain. Moreover, the mitochondrial-related apoptotic pathway is recognized as one of the primary mechanisms regulating apoptosis[3]. Therefore, we propose that a novel LA capable of mitigating inflammation-induced mitochondria-related nerve cell apoptosis may exhibit effective anesthetic properties under inflammatory conditions. However, there is currently no study demonstrating that commonly used LAs, including AT and lidocaine, can inhibit inflammation-induced mitochondria-related nerve cell apoptosis.

It is for this reason that we have undertaken the design of a novel local anesthetic, AT-17, which aims to mitigate such side effects by modifying the structure of existing anesthetics through computer simulation and artificial intelligence[4]. Firstly, we employed a groundbreaking molecular generation framework known as DeepSA, which utilized deep simulated annealing for structural modifications. This approach enabled the generation of over 400 analogs based on the structural foundation of AT, all of which met pre-defined criteria and demonstrated enhanced anti-inflammatory properties compared to AT. Among these candidates, one compound, AT-17, emerged as particularly promising. In comparison to traditional AT, AT-17 exhibited superior anesthetic efficacy, outperforming even AT in combination with epinephrine, which potentially reduces certain side effects associated with epinephrine supplementation, including cardiovascular risks. Additionally, AT-17 presented lower systemic and local toxicity levels, establishing it as a safer option at reduced concentrations for clinical applications. Most importantly, our studies indicated that AT-17 effectively attenuated inflammation in the complete Freund's adjuvant (CFA)-induced chronic inflammation model. Furthermore, AT-17 displayed an anti-inflammatory function through its capacity to ameliorate mitochondrial dysfunction. However, further investigation is warranted to elucidate whether AT-17 retains effective anesthetic properties under acute inflammatory conditions, including specifically oral acute inflammatory scenarios, and to clarify the underlying mechanisms involved.

Herein, we conducted a series of experiments, including rat formalin pain, carrageenan pain, oral extraction-induced inflammatory pain, and pulpitis models, to investigate the efficacy of AT-17 in various inflammatory conditions. Notably and significantly, we discovered that mitochondrial-related apoptosis plays a crucial role in the anesthetic properties of AT-17 within these inflammatory contexts. This finding holds substantial implications for future drug development as well as for enhancing our understanding of their mechanisms of action.

2. Materials and methods

2.1. Animals

Male Sprague−Dawley rats (Dossy Experimental Animal Company, Chengdu, China) aged 6−8 weeks and weighing 250−300 g were housed at 25 °C with free access to food and water under a 12-h light/12-h dark cycle. ICR mice (Dossy Experimental Animal Company, Chengdu, China) aged 30−40 days and weighing 20−30 g were housed under similar conditions. Animals were acclimated to the experimental environment and experimenter, and handled daily to minimize stress-induced analgesia. Animals were randomly assigned to groups. All behavioral tests were performed by experimenters blinded to the treatment received by each animal. All animal experiments were performed in compliance with the Agreement of the Experimental Animal Ethics Committee, West China Hospital of Stomatology, Sichuan University (Approval No. WCHSIRB-D-2023-570).

2.2. Rat plantar formalin pain and carrageenan pain

Rats were induced and maintained anesthetized by inhalation of 1% to 3% isoflurane, and 5% formalin and 1% carrageenan were injected into the right foot of each rat. After 48 h, it was observed that the soles of the feet were visibly swollen and the withdrawal threshold of the hind paw of the rats was significantly reduced as measured by the electronic Von Frey stimulator (ITCC, Los Angeles, CA, USA). The injected drugs were AT and AT-17, and the blank control was an equal dose of normal saline. The injection volume for each rat for treatment or control was 0.2 mL and was injected subcutaneously at the swollen site of the rat's foot. The electronic Von Frey stimulator was used to stimulate the side of the foot of the drug-injected rats to observe the effect of local anesthesia. The test was performed every 10 min after the onset of the effect, and the measured value was more than half of the

difference between the limb weight and the baseline as the onset of anesthesia, and less than or equal to the value was considered as the failure of anesthesia.

2.3. Rat inflammatory mandibular and maxillary teeth extractions models

Injecting 0.1 mL 2 mg/mL lipopolysaccharide (LPS) into the buccal side of the first molars of the upper and lower jaws in rats, the first molars were extracted after infiltration anesthesia and inferior groove nerve block anesthesia, respectively, to construct maxillary extraction inflammation rat model and mandibular extraction inflammation rat model. The first molar of the rat was exposed through the opening, and the neck of the first molar of the rat was clamped with curved vascular forceps. The first molar of the rat was dislocated by shaking the first molar to the lip and tongue. The residual root was removed by the dental probe, and then closed the gingiva after compression and hemostasis by 3-0 sutures. The facial scratching frequency in first 1 h, and the weight change, food intake, and water intake changes in the first three days were recorded[5].

2.4. Rat pulpitis model

The mouth opener remained open, the tongue was gently retracted using forceps, the mesial pulp angle of the mandibular first molar was exposed by an electric drill. Then, a cotton ball soaked in 2 mg/mL LPS in advance was placed in the pulp cavity, and the pulp opening was sealed with temporary sealing paste. The facial scratching frequency in first hour, and the weight change, food intake, and water intake changes in the first three days were recorded.

2.5. Cell culture and reagents

DRG neurons from male rats weighing 180−200 g were dissociated and cultured as described previously. In brief, rats were sacrificed by spinal cord dislocation method. Then, ganglia were quickly excised and placed in ice-cold Hanks' Balanced Salt Solution (HBSS; Gibco, NY, USA). After removing the connective tissue gently, the ganglia were sequentially digested with 2 mL collagenase IV (2 mg/mL) followed by 2 mL trypsin (10 mg/mL) for 30 min in an incubator. After termination of digestion *via* fetal bovine serum (FBS; Corning, NY, USA), DRG neurons suspension was obtained by filtration. Then, cells were inoculated in petri dishes pre-treated with poly-L-lysine (Sigma−Aldrich, St. Louis, MO, USA) at 37 °C for 1 h. DRG neurons were grown in Neurobasal (Gibco, USA) supplemented with 10% of FBS, 1% penicillin−streptomycin solution (Gibco, USA) and B27 supplement (Thermo Fisher Scientific, MA, USA). PC12 cells were obtained from the Conservation Genetics CAS Kunming Cell Bank (No. KCB200735YJ). Cells were cultured in the F12K medium (Gibco, USA) supplemented with 10% horse serum (Gibco, USA) and 5% FBS. To induce their differentiation, PC12 cells were poly-L-lysine-coated plates in the medium supplemented with mouse β-NGF (50 ng/mL; Sino Biological, Beijing, China).

2.6. Flow cytometry analysis (FC)

Flow cytometry using the Annexin V-FITC Apoptosis Detection Kit (Invitrogen) was for the test of cell apoptosis. Treated cells were seeded in 6-well plates and digested after 48 h. Then, cells were resuspended with 1 × Binding Buffer. Stained with 5 μL of Annexin V-FITC Conjugate and 5 μL of Propidium Iodide Solution, cells were incubated for 30 min at room temperature under dark conditions. After washing and resuspending, the percentage of stained cells was analyzed using a FACScalibur (Becton-Dickinson). Experiments were conducted in triplicate.

2.7. qRT-PCR

Total RNA of cells was extracted *via* Trizol. The reverse transcription was carried out following the manufacturer's procedure using HiScript III 1st Strand cDNA Synthesis Kit (gDNA wiper) (Vazyme, R312, Nanjing, China). Then qRT-PCR was performed with on ABI PRISM 7900 sequence detection system. Reaction system: 12 μL DEPC water, 4 μL 5 × BlazeTaq qPCR Mix, 1 μL Forward Primer (10 μmol/L), 1 μL Reverse Primer (10 μmol/L), 2 μL template cDNA, final volume was 20 μL. Reaction conditions: 95 °C 30 s → (95 °C 10 s → 60 °C 30 s) × 40 cycles. Specific primers of each gene for qRT-PCR were shown as Supporting Information Table 1. All experiments were repeated at least three times and the relative expressions of detected genes were calculated *via* $2^{-\Delta\Delta CT}$ method.

2.8. Westing bolt

Total proteins of tissue specimens were prepared *via* RIPA lysis buffer. Next, proteins were separated through sodium dodecyl sulfate−polyacrylamide gel electrophoresis. Then, gel was transferred onto a PVDF membrane (Millipore, Boston, MA, USA). After blocked in 5% defatted milk for 2 h, membranes were incubated with specific primary antibody overnight at 4 °C. After incubating goat anti-rabbit or goat anti-mouse secondary antibody (MultiSciences, Hangzhou, China), membranes with target protein incubated with the chemiluminescence reagent (Yamei Biotechnology, Shanghai, China) were visualized *via* ChemiDoc XRS + System (Bio-Rad, Hercules, CA, USA). The antibodies were used as Supporting Information Table 2.

2.9. Immunofluorescence (IFC)

Cells were seeded on the poly-L-lysine−coated slides. For 8-OHdG staining, cells were firstly incubated with MitoTracker Deep Red (500 nmol/L; Beyotime, Shanghai, China) at 37 °C for 20 min, fixed with methanol and then treated with 0.2% Triton X-100 (Sigma−Aldrich, MO, USA) to increase cell membrane penetrability. Cells were incubated with CytC (1:250; Proteintech, Chicago, USA) at 4 °C overnight and then incubated with goat anti-mouse IgG H&L/AF488 secondary antibodies (1:500; Bioss, Beijing, China) for 1 h at room temperature. Nuclei were stained with 4′,6-diamidino-2-phenylindole (DAPI) (Boster, Wuhan, China) for 20 min. Immunofluorescence images were acquired by confocal laser scanning microscopy.

2.10. Electrophysiology whole-cell mode voltage clamp detection

Microelectrode resistance 3−5 MΩ. The in-electrode liquid (K-gluconate 125 mmol/L, NaCl 10 mmol/L, $CaCl_2$ 1.5 mmol/L, EGTA 5 mmol/L, $MgCl_2 \cdot 6H_2O$ 1 mmol/L, HEPES 10 mmol/L, glucose 10 mmol/L). Adjust pH to 7.35−7.45. The outer solution contained 120 mmol/L NaCl, 5 mmol/L KCl, 1 mmol/L $CaCl_2$,

1.5 mmol/L $MgCl_2$, 10 mmol/L HEPES, and 10 mmol/L glucose, adjust pH to 7.3 with NaOH. The osmotic pressure of all solutions was 300−330 mOsm. All records were taken at room temperature. We recorded the sodium current track in voltage clamp mode (clamp potential −70 mV), the voltage was depolarized from −70 to 0 mV, and the stimulation time was 50 ms. Then detected the magnitude of the sodium current. Signal was amplified by a Multi Clamp 700B amplifier, filtered at 10 kHz, and converted by an Axon Digidata 1440 A digital-to-analog/analog-to-digital converter at a sampling frequency of 10 kHz.

2.11. Statistics

Data are presented as means ± standard error of mean (SEM). Differences in the mean between the two groups were analyzed using Student's *t*-test for normally distributed data. To compare means between more than two groups, a one-way analysis of variance (ANOVA) with *post hoc* (Tukey) for normally distributed data. Statistical analysis, as indicated in each figure legend, was performed using GraphPad Prism software v9.4.1. Data are expressed as mean ± SEM; $*P < 0.05$, $**P < 0.01$, and $***P < 0.001$. $P > 0.05$ was considered to be statistically significant.

3. Results

3.1. AT-17 played an effective role in acute and oral inflammation models

Our previous study demonstrated that AT-17 exhibited a more satisfactory effect than AT in both the rat plantar CFA-induced chronic inflammation model and the plantar incision pain model. Moreover, we investigated the roles of AT-17 in acute inflammation and oral inflammation models (Fig. 1A).

We conducted rat plantar formalin pain and carrageenan-induced pain models to evaluate the efficacy of AT-17 in acute inflammation. The formalin-induced pain was measured from 15 to 20 min post-injection, representing a type of peripheral inflammatory pain associated with spinal cord sensitization, which allowed us to examine the impact of AT-17. The results indicated (Fig. 1B) that both AT-17 and AT were capable of increasing the diminished paw contraction threshold caused by formalin injection. Notably, administration of AT-17 alleviated pain for a duration ranging from 40 to 50 min, whereas the analgesic effect of AT lasted only 10 to 20 min. Additionally, the area under curve (AUC), reflecting the anesthetic efficacy of AT-17, was significantly greater than that observed with AT ($P < 0.05$). In the carrageenan-induced pain model (Fig. 1C), relief provided by AT-17 extended from 90 to 100 min, exceeding that offered by AT (60 to 70 min; $P < 0.05$). Furthermore, AUC values for AT-17 surpassed those for AT ($P < 0.05$). It is noteworthy that while AT appeared effective at mitigating carrageenan-induced discomfort—consistent with clinical observations—it may have been influenced by our timing: we injected AT shortly after administering carrageenan when its analgesic effects might not have fully manifested; typically, peak discomfort arises around 5 h post-carrageenan injection in rats. The findings derived from these two inflammatory pain models strongly suggest that AT-17 consistently exhibits superior effectiveness within acute inflammatory contexts compared to AT.

The oral inflammation models were then established. Following the injection of 0.1 mL of LPS at a concentration of 2 mg/mL into the buccal vestibular sulcus adjacent to the right mandibular and maxillary first molars in rats, tooth extractions were performed, as confirmed by MicroCT imaging (Supporting Information Fig. S1A and S1B). When comparing the rats that received PBS injections before tooth extraction (NC group) with those injected with LPS (LPS group), the latter exhibited significantly more pronounced short-term pain, indicated by the number of facial scratches observed within 30 min after awakening ($P < 0.05$), as well as long-term pain characterized by variations in body weight, water intake, and food consumption over three days ($P < 0.05$). This finding was consistent with the considerable intraoperative and postoperative pain experienced by patients undergoing acute inflammatory mandibular and maxillary teeth extractions in clinical settings. Furthermore, the inflammatory pain associated with mandibular tooth extraction persisted for up to three days, peaking on Days 1 and 2 (Fig. S1A). In contrast, inflammatory pain following maxillary tooth extraction lasted for two days and was most pronounced on Day 1 only (Fig. S1B).

The efficacy of AT-17 in oral inflammation models was subsequently investigated. In inflammatory mandibular and maxillary tooth extraction models, 0.2 mL AT-17 and AT with a concentration of 2% were administered through inferior alveolar nerve block anesthesia and infiltration anesthesia, respectively. In the model of inflammatory mandibular tooth extractions, AT-17 demonstrated a superior ability to reduce the frequency of facial scratches in rats after 30 min of wakefulness compared to AT ($P < 0.05$). Furthermore, on both the first and second days post-treatment, AT-17 significantly mitigated weight loss as well as decreased water and food intake induced by LPS, outperforming AT (Fig. 1D and Fig. S1C, $P < 0.05$). Regarding the inflammatory maxillary tooth extraction model, the incidence of facial scratches in the AT-17 group was notably lower than that observed in the AT group ($P < 0.05$). On day one post-treatment, AT-17 also improved outcomes related to weight loss and reduced food intake ($P < 0.05$), whereas improvements with AT were not statistically significant (Fig. 1E and Fig. S1D, $P > 0.05$). Concerning the pulpitis model, both AT and AT-17 treatments were effective in reducing facial scratching occurrences 30 min following anesthetic administration ($P < 0.05$), showing similar efficacy potentially due to insufficient development of acute pulpitis upon awakening from anesthesia[6]. Additionally, on day one following treatment for pulpitis-induced conditions, AT-17 significantly enhanced recovery from weight loss as well as increased water intake and food consumption ($P < 0.05$), while changes associated with treatment using AT did not yield statistically significant results (Fig. 1F, $P > 0.05$). Collectively, these findings suggested that AT-17 possessed effective anesthetic properties within rat models characterized by acute plantar inflammation alongside oral extraction inflammation models and pulpitis scenarios, indicating that AT-17 provided enhanced analgesic efficacy under inflammatory conditions, which demonstrated superior performance relative to classical treatment options such as AT.

3.2. Nerve cells apoptosis influenced the role of AT-17 in inflammatory mandibular teeth extraction model

We further evaluated the role of nerve apoptosis in an inflammatory mandibular teeth extraction model, as observed in inflammatory pain[7] and neuropathic pain models[8]. Inferior alveolar nerves from various treatment groups were collected for TUNEL staining to assess nerve apoptosis. After 1 h of treatment, no significant differences were noted in TUNEL staining intensity or the ratio of positive cells among the three groups. In comparison

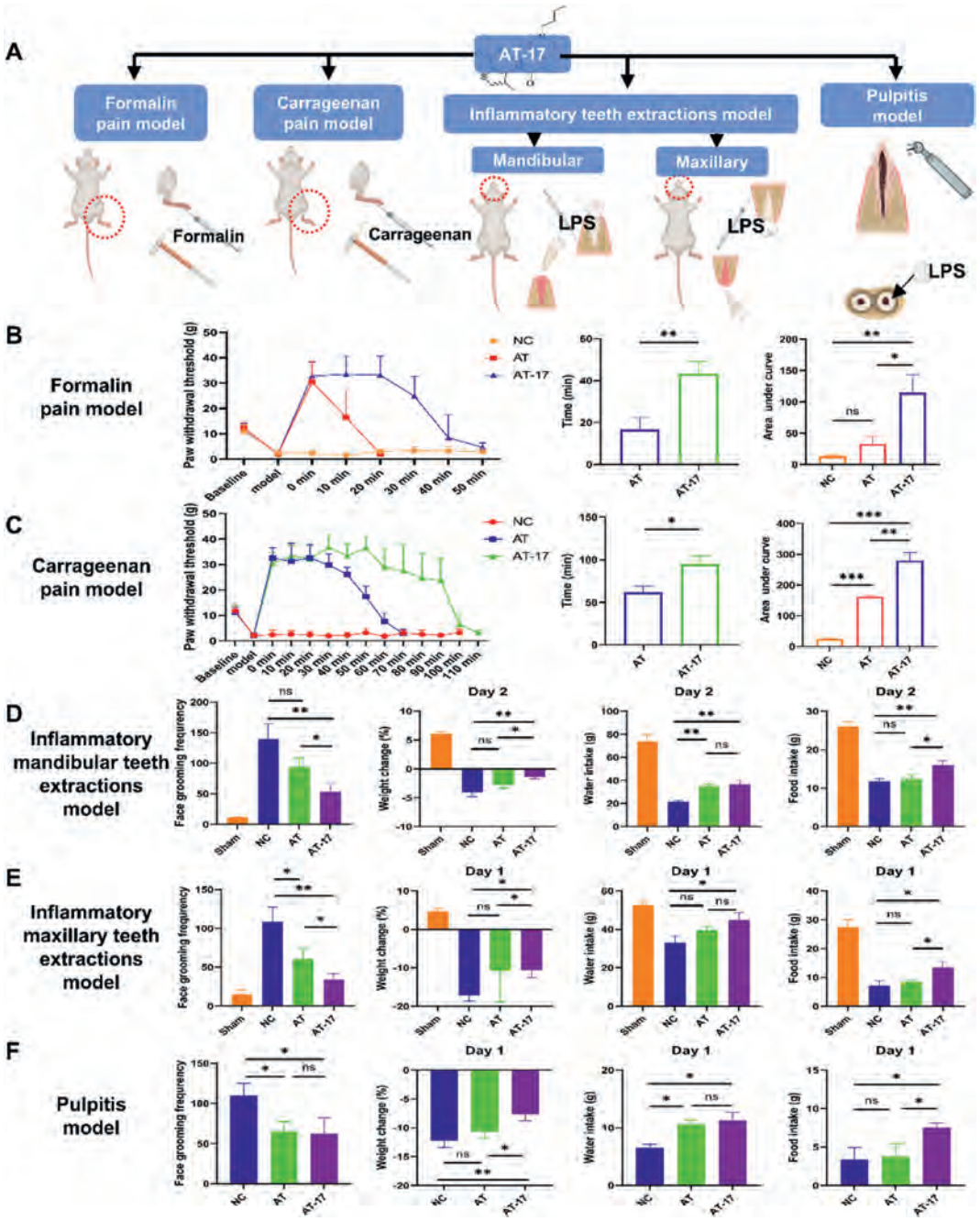

Figure 1 The role of AT-17 in rat inflammatory models. (A) The schematic diagram of animal experiments. (B) The role of AT-17 in rat formalin pain model ($n = 6$). (C) The role of AT-17 in rat carrageenan pain mode ($n = 6$). (D) The role of AT-17 in rat inflammatory mandibular teeth extractions model ($n = 6$). (E) The role of AT-17 in rat inflammatory maxillary teeth extractions model ($n = 6$). (F) The role of AT-17 in rat pulpitis model ($n = 6$). Data are presented as mean ± SEM. $^{*}P < 0.05$, $^{**}P < 0.01$, $^{***}P < 0.001$, and ns $P > 0.05$.

to the NC group, both the staining intensity and the ratio of positive cells in inferior alveolar nerve tissues treated with AT-17 for 2 days were significantly diminished; however, no significant difference was found between the NC and AT groups (Fig. 2A). These results suggested that the long-term analgesic effect of AT-17 in the mandibular extraction inflammation model may be linked to nerve apoptosis, while its short-term analgesic effect appeared unrelated to this process.

As demonstrated in our previous studies, AT-17 had the potential to enhance mitochondrial function in nerve cells within an inflammatory environment. This improvement was crucial for modulating the regulation of endogenous apoptotic pathways in cells. To assess the impact of mitochondria-related nerve apoptosis on alleviating pain associated with the extraction of inflamed mandibular teeth following AT-17 administration, we injected ABT-737, a mitochondrial apoptotic pathway activator, into the inferior alveolar nerve one day prior to performing an AT-17 nerve block. Compared to the group received only the AT-17 nerve block, pre-treatment with ABT-737 resulted in a significant increase in facial scratching frequency during the first 30 min post-

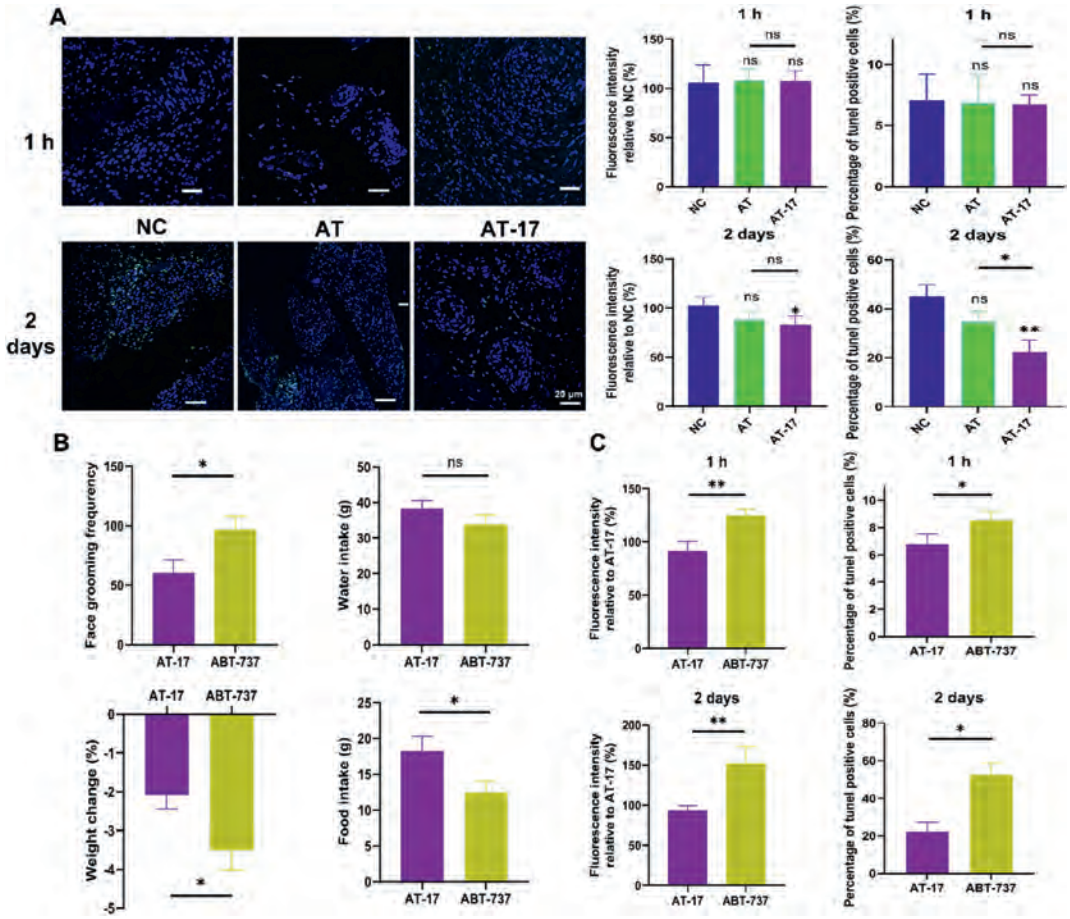

Figure 2 The role of nerve cells apoptosis in inflammatory teeth extraction pain. (A) TUNEL staining of the inferior alveolar nerve tissue from rats after extraction of inflamed mandibular teeth for 1 h and 2 days. (B) The role of ABT-737 in AT-17 influencing pain of rats after tooth extraction on Day 2 ($n = 6$). (C) TUNEL staining results of inferior alveolar nerve tissue in the ABT-737 group ($n = 6$). Data are presented as mean ± SEM.*$P < 0.05$, **$P < 0.01$, ***$P < 0.001$, and ns $P > 0.05$.

intervention and exacerbated weight loss along with decreased food intake observed on Day 2 (Fig. 2B). Furthermore, tissues from the inferior alveolar nerves treated with ABT-737 exhibited markedly elevated TUNEL staining intensity and a higher ratio of positive cells after 1 h and two days of treatment (Fig. 2C). These findings suggested that mitochondria-related nerve apoptosis played a substantial role in mediating both short-term and long-term pain relief provided by AT-17 following inflammatory tooth extractions in rats.

3.3. AT-17 inhibited the LPS-induced mitochondria-related apoptosis of never cells

To evaluate the regulatory effect of AT-17 on apoptosis in inflammatory nerve cells, we developed both chronic inflammatory nerve cell models (LPS(pre) + drug) and acute inflammatory nerve cell models (LPS(co) + drug), as previously described. Under these conditions, LPS exposure significantly increased DRG apoptosis, whereas AT-17 markedly reduced cell apoptosis following LPS stimulation. This effect was notably more effective than that observed with AT treatment alone (Fig. 3A). TUNEL staining corroborated these findings (Supporting Information Fig. S2A).

We further investigated whether the inhibition of nerve cell apoptosis by AT-17 was directly linked to mitochondrial function. Following LPS stimulation, the expression levels of pro-apoptotic factors (CASPASE3, CASPASE7, CASPASE9, and BAX) in nerve cells were found to be upregulated, while the expression of the anti-apoptotic factor BCL2 was downregulated (Fig. 3B and Fig. S2B). Notably, AT-17 effectively inhibited the effects of LPS across both inflammation models, indicating that it may mitigate LPS-induced neuronal apoptosis *via* the mitochondrial pathway. Furthermore, qRT-PCR was used to test the mRNA expressions of 13 genes encoded by mtDNA (*Nd1*, *Nd2*, *Nd3*, *Nd4*, *Nd4l*, *Nd5*, *Nd6*, *Mtco1*, *Mtco2*, *Mtco3*, *Ctyb*, *Atp6*, and *Atp8*) and 7 mitochondrial-related genes encoded by nuclear DNA (*Nduf3*, *Sdha*, *Uqcrc2*, *Hig2*, *Atp5b*, *Top1m* and *Tfam*). The results suggested that AT-17 can partially restore these downregulated gene expressions observed in both inflammation models (Supporting Information Fig. S3). Furthermore, AT-17 can also upregulate the expression of TOMM20, a marker indicative of mitochondrial quality (Fig. 3B and Fig. S2B). In addition, regarding the effects on mitochondrial morphology, AT-17 was found to reverse the reduction of the average branch length of mitochondria induced by LPS, as demonstrated by Mito-tracker staining results (Fig. 3C and Fig. S2C, $P < 0.05$). And AT-17 not only ameliorated severe structural damage to mitochondria caused by LPS, evidenced by wrinkling, swelling, roundness, and disruption or loss of mitochondrial cristae, but also restored reductions in mitochondrial

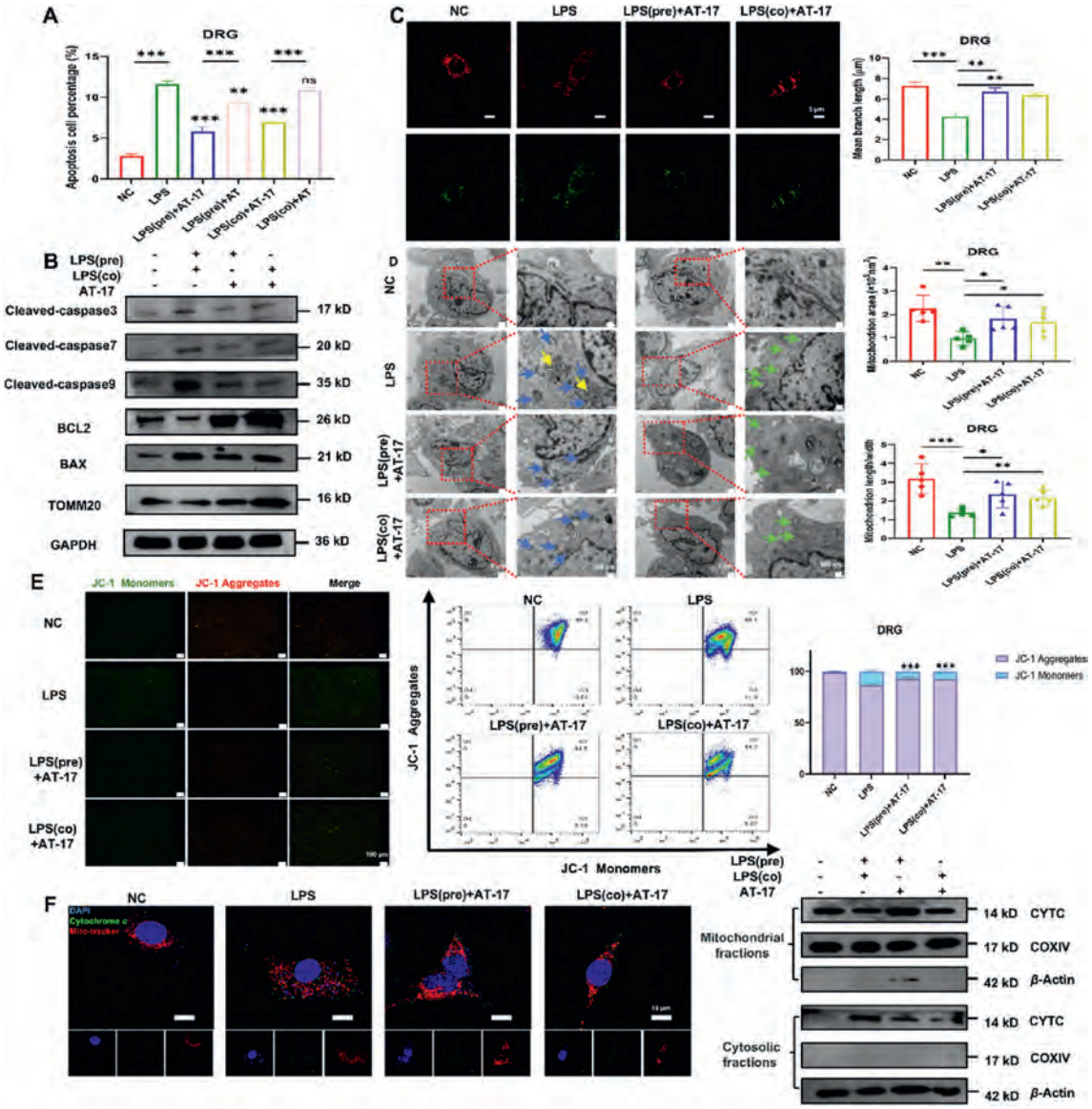

Figure 3 The role of AT-17 in LPS-stimulated DRG apoptosis and mitochondrial function. (A) The role of AT-17 in DRG apoptosis ($n = 3$). (B) The role of AT-17 in the mitochondrial-related apoptosis factors and TOMM20 expressions of DRG. (C) Mito-tracker staining explores the role of AT-17 in the mitochondrial cytoskeleton of DRG ($n = 5$). (D) TEM tests the role of AT-17 in the mitochondrial structure of DRG (bule arrow: wrinkling mitochondria; green arrow: swelling mitochondria; yellow arrow: autophagosome. $n = 5$). (E) The role of AT-17 in the MMP of DRG (left: IFC; middle and right: FC. $n = 3$). (F) The role of AT-17 in the CYTC release of DRG (left: IFC; right: WB). Data are presented as mean ± SEM. $^*P < 0.05$, $^{**}P < 0.01$, $^{***}P < 0.001$, and ns $P > 0.05$.

area and aspect ratio (Fig. 3D and Fig. S2D, $P < 0.05$). Additionally, apoptotic bodies were observed in DRG treated with LPS; however, no apoptotic bodies were detected in the other experimental groups (Fig. S2E). Moreover, during the process of mitochondria-related cell apoptosis, a decrease in mitochondrial membrane potential (MMP) was noted, which was beneficial for reducing the early stages of cell apoptosis. Notably, mitochondrial outer membrane permeabilization (MOMP) occurred concurrently with this process, which facilitated the release of cytochrome *c* (CYTC) from mitochondria into the cytoplasm[9]. Predictably, AT-17 was able to mitigate both MMP reduction (Fig. 3E and Fig. S2F) and CYTC release (Fig. 3F and Fig. S2G). Collectively, these data indicated that AT-17 effectively improved mitochondrial dysfunction in nerve cells within both chronic and acute inflammatory models to inhibit cell apoptosis.

3.4. AT-17 decreased mtROS generation to contribute to its anti-apoptosis effect

Our previous results demonstrated that AT-17 could decrease the generation of mitochondrial reactive oxygen species (mtROS) induced by LPS, which contributed to the inhibition of NLRP3 inflammasome activation and IL1β release[4]. Given the crucial role of mtROS in regulating mitochondrial function, we subsequently employed tert-butyl hydroperoxide (T-BHP), a ROS inducer, alongside mito-TEMPO (MT), a mtROS scavenger, to investigate the role that mtROS played in mediating the anti-apoptotic effects of AT-17. As illustrated by flow cytometry, T-BHP not only augmented LPS's effect on promoting neuronal apoptosis but also mitigated the protective effects of AT-17 against neuronal cell death (Fig. 4A and Supporting Information Fig. S4A). Likewise,

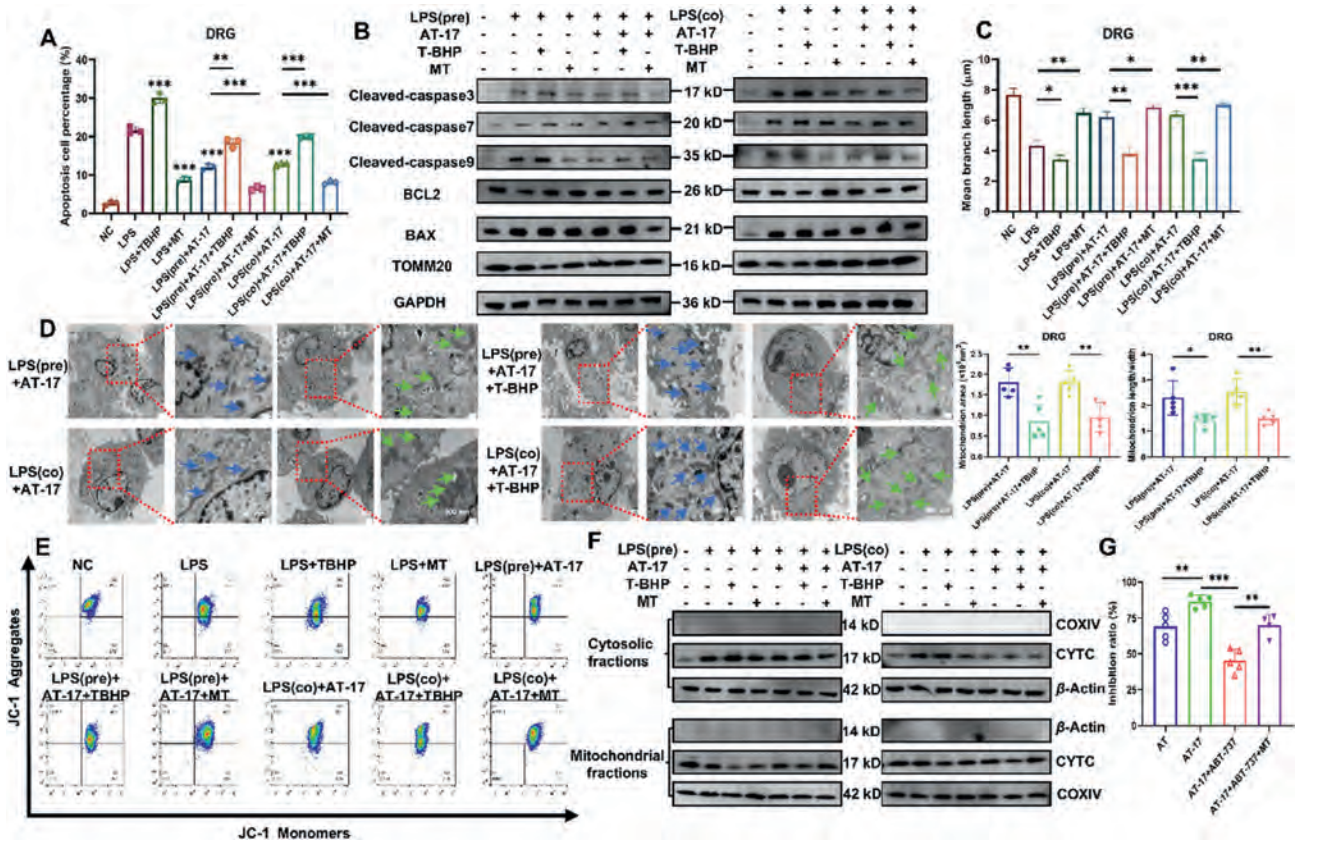

Figure 4 The role of mtROS in AT-17 inhibiting LPS-stimulated DRG apoptosis and improving mitochondrial dysfunction. (A) The role of mtROS in AT-17 inhibiting DRG apoptosis ($n = 3$). (B) The role of mtROS in AT-17 influencing mitochondrial-related apoptosis factors and TOMM20 expressions of DRG. (C) Mito-tracker staining explores the role of mtROS in AT-17 influencing mitochondrial cytoskeleton of DRG ($n = 5$). (D) TEM tests the role of mtROS in AT-17 influencing mitochondrial structure of DRG ($n = 5$). (E) The role of mtROS in AT-17 influencing MMP of DRG. (F) The role of mtROS in AT-17 influencing CYTC release of DRG. (G) The role of mtROS in AT-17 influencing Na_V currents of LPS-stimulated DRG *via* whole-cell patch clamp techniques ($n = 6$). Data are presented as mean ± SEM. $^*P < 0.05$, $^{**}P < 0.01$, $^{***}P < 0.001$.

T-BHP was able to reverse AT-17's impact on endogenous apoptotic factors such as CASPASE3, CASPASE7, CASPASE9, BAX, and BCL2 as well as on TOMM20 (Fig. 4B and Fig. S4B). Moreover, MT exhibited contrasting effects compared to T-BHP, indicating that AT-17's modulation of mitochondrial-related protein expression was associated with mtROS generation. Subsequently, treatment with T-BHP resulted in fragmentation of the improved mitochondrial network induced by AT-17 into shorter rod-like or spherical structures (Fig. 4C and Fig. S4C). This remodeling exacerbated structural damage to mitochondria as evidenced by significant alterations in area and aspect ratio (Fig. 4D). Consistently, the functionality of AT-17 regarding decreases in MMP was inhibited by T-BHP, while being promoted by MT (Fig. 4E and Fig. S4D). Additionally, CYTC release, signifying MOMP, was altered similarly, suppressed by T-BHP and enhanced through MT treatment (Fig. 4F and Fig. S4E). In conclusion, our findings suggested that AT-17-mediated attenuation of mtROS signaling may serve as an upstream factor ameliorating mitochondrial dysfunction, thereby inhibiting cell apoptosis.

Then, we aimed to investigate whether the anti-apoptotic effect of AT-17 contributed to its anesthetic properties. Utilizing whole-cell patch clamp techniques, we examined the effects of AT and AT-17 on sodium channels, key targets in local anesthesia, in inflamed DRG pretreated with LPS for 5 h. The inhibition rate of voltage-gated sodium channel (Na_V) currents in inflamed DRG following treatment with AT-17 was significantly higher, compared to that observed after the same concentration of AT treatment, indicating a stronger anesthetic effect. Therefore, the superior analgesic efficacy of AT-17 in inflammatory animal models was partly attributable to its more pronounced anesthetic action. However, pretreatment with ABT-737 disrupted the inhibitory effect of AT-17 on Na_V currents, suggesting that mitochondrial-related apoptosis may modulate the anesthetic properties of AT-17. Furthermore, MT treatment enhanced the inhibitory function of AT-17 on Na_V currents, highlighting the crucial role of mtROS (Fig. 4G and Supporting Information Fig. S5A−S5D). Additionally, we explored whether AT-17 primarily acted through $Na_V1.7$ or $Na_V1.8$, the principal targets for local anesthetics. In two inflammatory cell models, treatment with AT-17 restored the expression levels of $Na_V1.7$, but did not have a significant impact on the recovery of $Na_V1.8$ (Fig. S5E). In summary, our findings suggested that AT-17 may reduce mtROS generation in inflamed DRG cells to mitigate cell apoptosis and thereby enhance its anesthetic effectiveness, with $Na_V1.7$ likely playing a pivotal role.

3.5. AT-17/mtROS activated the Nrf2 pathway to inhibit never cells' apoptosis caused by LPS

As mtROS mediated the influence of AT-17 on mitochondrial-related apoptosis, the genes involved in mitochondrial function were likely regulated by mtROS, including peroxisome proliferator-activated receptor gamma coactivator 1-alpha (*Pgc1a*), nuclear factor erythroid 2-related factor 2 (*Nrf2*), mitochondrial transcription factor A (*Tfam*), mitochondrial DNA topoisomerase I (*Top1m*), peroxisome proliferator-activated receptor gamma coactivator 1-beta (*Pgc1b*), mitochondrial transcription factor B1 (*Tfbm1*), mitochondrial transcription factor B2 (*Tfbm2*), transient receptor potential cation channel subfamily M member 2 (*Trpm*), and brain-derived neurotrophic factor (*Bdnf*)[10]. Following LPS stimulation, the mRNA levels of these eight mitochondrial biological factors demonstrated a marked decrease. AT-17 was found to upregulate the expression of certain factors in two inflammation models, specifically *Tfam*, *Top1m*, *Pgc1a*, and *Nrf2*, while only the expressions of *Pgc1a* and *Nrf2* were decreased after T-BHP treatment. This indicated that PGC1α and NRF2 may serve as downstream targets regulated by AT-17/mtROS (Supporting Information Fig. S6A). Subsequently, we assessed the roles of PGC1α and NRF2 in mediating the anti-apoptotic effect exerted by AT-17/mtROS. Both PGC1α agonists (ZLN005) and NRF2 agonists (TBHQ) were able to partially counteract DRG cell apoptosis following LPS + AT-17+T-BHP treatment; however, TBHQ exhibited a more pronounced recovery effect than ZLN005 (Fig. 5A). These findings suggested that NRF2 played a significant role in attenuating nerve cell apoptosis induced by AT-17.

We further observed that AT-17 could upregulate the expressions of NRF2, HO1, and NQO1, while downregulating KEAP1 expression in LPS-stimulated nerve cells. This effect could be reversed by T-BHP treatment (Fig. 5B and Fig. S6B). To confirm the necessity of NRF2 for the anti-apoptotic effects of AT-17, TBHQ was administered to nerve cells treated with LPS + AT-17+TBHP. As anticipated, the increased expressions of CASPASE3, CASPASE7, CASPASE9, and BAX induced by AT-17/T-BHP were significantly impaired by TBHQ treatment; conversely, reductions in BCL2 and TOMM20 expressions were also noted (Fig. 5C). Additionally, TBHQ treatment effectively suppressed activation of the NRF2 pathway in nerve cells following LPS + AT-17+T-BHP treatment as evidenced by decreased expression levels of KEAP1 alongside increased levels

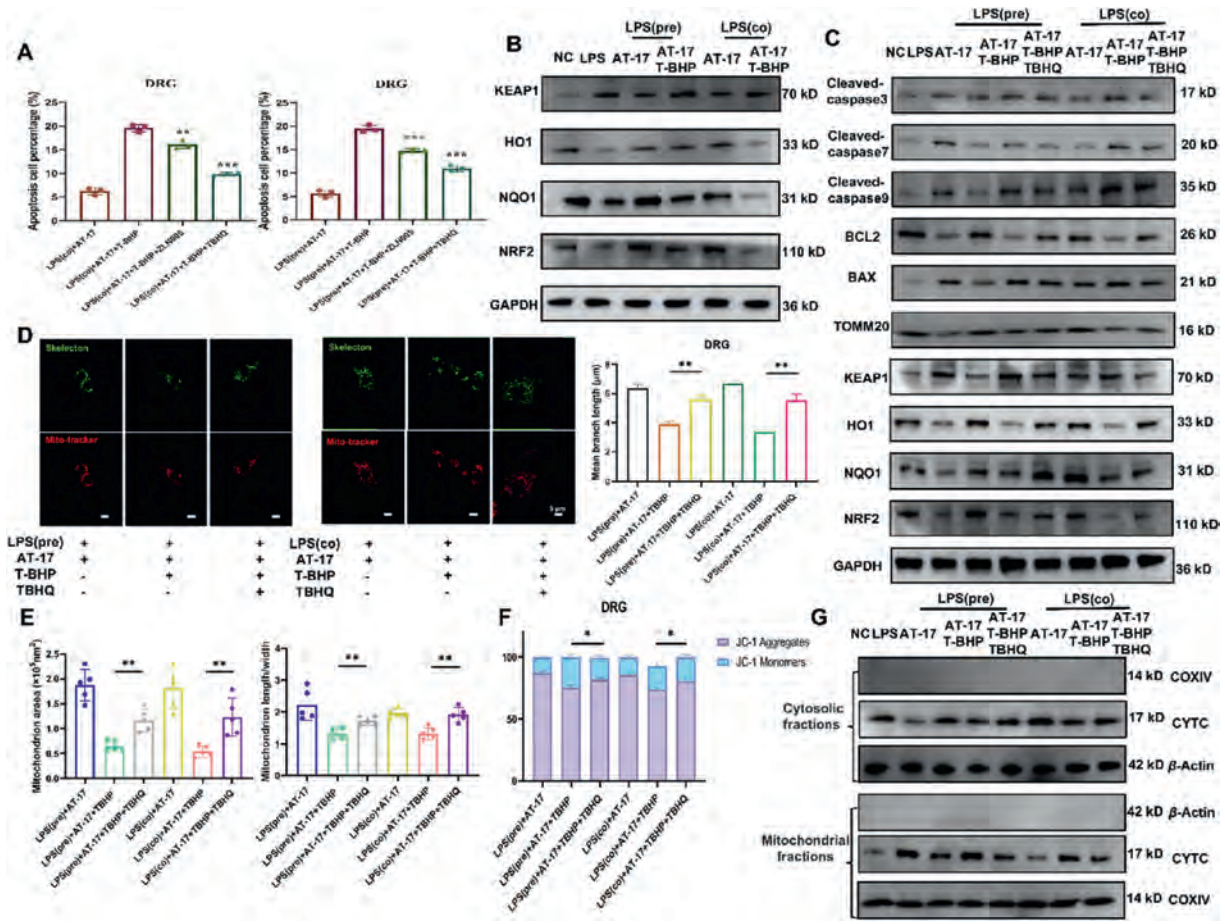

Figure 5 The role of NRF2 in AT-17/mtROS influencing LPS-stimulated DRG apoptosis and mitochondrial dysfunction. (A) The role of NRF2 in AT-17/mtROS inhibiting DRG apoptosis ($n = 3$). (B) The role of mtROS in AT-17 influencing the NRF2 pathway. (C) The role of NRF2 in AT-17/mtROS influencing mitochondrial-related apoptosis factors, TOMM20, and the NRF2 pathway expressions of DRG. (D) MitoTracker staining explores the role of NRF2 in AT-17/mtROS influencing mitochondrial cytoskeleton of DRG ($n = 5$). (E) TEM tests the role of NRF2 in AT-17/mtROS influencing mitochondrial structure of DRG ($n = 5$). (F) The role of NRF2 in AT-17/mtROS influencing MMP of DRG ($n = 3$). (G) The role of NRF2 in AT-17/mtROS influencing CYTC release of DRG. Data are presented as mean ± SEM. $^*P < 0.05$, $^{**}P < 0.01$, $^{***}P < 0.001$.

of NRF2, HO1 and NQO1 (Fig. 5C). Furthermore, T-BHP-induced mitochondrial damage was partially restored upon TBHQ administration, including an increase in mean branch length of mitochondria (Fig. 5D and Fig. S6C) and improved overall mitochondrial structure (Fig. 5E). Consequently, features associated with mitochondrial-related apoptosis were diminished following TBHQ treatment, including reduced MMP levels (Fig. 5F and Fig. S6D), alongside enhanced CYTC expression within mitochondria and decreased presence in the cytoplasm (Fig. 5G). Therefore, these findings suggested that AT-17 can inhibit mtROS production in LPS-stimulated nerve cells while activating the NRF2 pathway to ameliorate mitochondrial dysfunction caused by LPS stimulation and inhibit neuronal apoptosis.

3.6. AT-17 inhibited the production of mtROS via Na^+/NCLX/ETC

It has been shown that Na^+ not only serves as the main mechanism by which LAs exert their anesthetic capacity on nerve cells, but also acts as a secondary messenger in cells to affect the activity of the electron transfer reaction (ETC) and modulate the production of ROS[11]. Consequently, we sought to investigate whether the inhibitory effect of AT-17 on mtROS is associated with the regulation of Na^+ concentration. As illustrated by the CoroNa Green fluorescent probe, AT-17 was able to inhibit the increase in intracellular Na^+ levels in nerve cells induced by LPS stimulation; however, this inhibitory effect of AT-17 was not markedly observed (Fig. 6A and Supporting Information Fig. S7A).

To further detect the effect of Na^+ concentration on AT-17 inhibition of mtROS production, we introduced varying concentrations of NaCl into the culture medium. As the concentration of NaCl increased, both Na^+ levels and mtROS production in LPS-stimulated nerve cells were elevated (Fig. 6B and C, Fig. S7B and S7C), indicating a positive correlation between AT-17's role in modulating mtROS production and intracellular Na^+ concentration. Furthermore, supplementation with NaCl was found to reverse AT-17's beneficial effect on reducing mitochondrial Na^+ levels in LPS-stimulated nerve cells (Fig. 6D and Fig. S7D). Since ETC is the major site to produce mtROS, we then explored the relationship between the role of AT-17 on ETC and the function of Na^+ concentration. Notably, AT-17 not only enhanced the expression levels of subunits I–IV of ETC proteins (Fig. 6E and Fig. S7E) but also restored activities of CI and CIII, which are widely regarded as crucial sites for mtROS production. However,

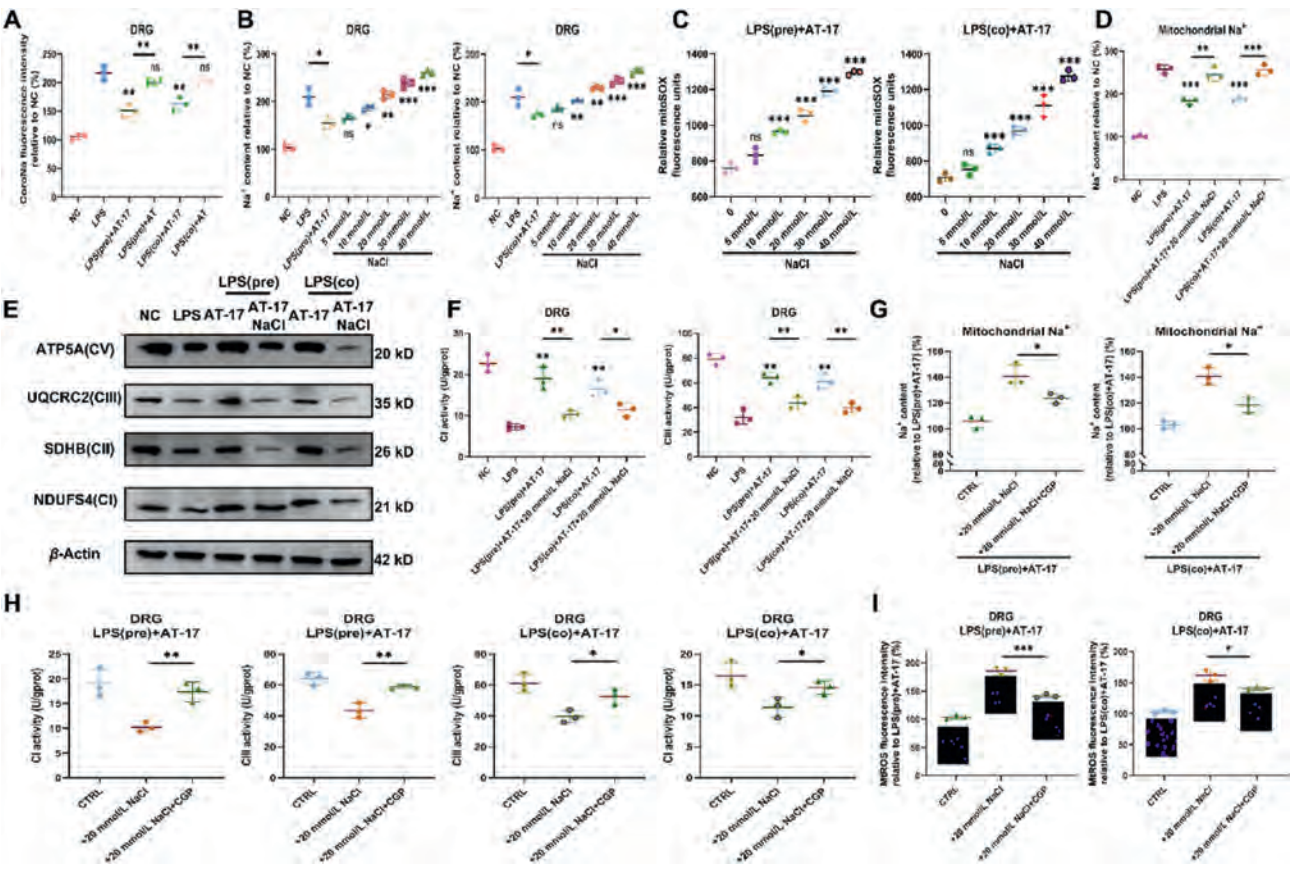

Figure 6 The mechanism of AT-17 inhibiting the mtROS production of LPS-stimulated DRG. (A) The role of AT-17 in the intracellular Na^+ concentration of DRG ($n = 3$). (B) The role of NaCl concentration in the intracellular Na^+ concentration of DRG ($n = 3$). (C) The role of NaCl concentration in the mtROS production of DRG ($n = 3$). (D) The role of 20 mmol/L NaCl in the mitochondrial Na^+ concentration of DRG ($n = 3$). (E) The role of 20 mmol/L NaCl in ETC subunit proteins expressions of DRG. (F) The role of 20 mmol/L NaCl in CI and CIII activities of LPS-stimulated DRG ($n = 3$). (G) The role of CGP-37157 in mitochondrial Na^+ concentration of DRG ($n = 3$). (H) The role of CGP-37157 in CI and CIII activities of DRG ($n = 3$). (I) The role of CGP-37157 in mtROS production of DRG ($n = 3$). Data are presented as mean ± SEM. $^*P < 0.05$, $^{**}P < 0.01$, $^{***}P < 0.001$, and ns $P > 0.05$.

additional supplementation with NaCl reversed these beneficial effects conferred by AT-17 on CI and CII activities (Fig. 6F and Fig. S7F). This suggested that AT-17's influence on mtROS production was closely related to both intracellular Na^+ concentration and ETC activity.

Further, we investigated the influence of mitochondrial Na^+/Ca^{2+} exchanger (NCLX), which regulated Na^+ influx into mitochondria on AT-17 function. CGP-37157, a specific inhibitor of NCLX, can reduce the increased mitochondrial Na^+ concentration caused by additional NaCl supplementation (Fig. 6G and Fig. S7G). And CGP-37157 expectedly restored the added NaCl-induced CI and CIII activities decrease (Fig. 6H and Fig. S7H) and mtROS production increase (Fig. 6I and Fig. S7I). Taken all together, these results suggested that AT-17 may lower LPS-stimulated Na^+ concentrations, subsequently decreasing mitochondrial Na^+ levels *via* NCLX; this sequence ultimately contributed to the restoration of CI and CIII activities and the inhibition of mtROS production.

4. Discussion

Most previous research has suggested that mitochondrial-related apoptosis is closely related to the toxicity of LA. Treatments with lidocaine and bupivacaine have been shown to induce mitochondrial dysfunction and subsequent mitochondrial-related apoptosis in nerve cells, skeletal muscle, and myocardial cells, ultimately resulting in neurotoxicity[12], muscle toxicity[13], and cardiac toxicity[14]. However, it is noteworthy that the mitochondrial dysfunction caused by LA may not solely represent a disadvantage. Lidocaine has been found to alleviate cognitive impairment induced by isoflurane in aged rats through mechanisms involving the reversal of mitochondrial dysfunction, restoration of MMP, amelioration of alterations in ETC activity brought on by isoflurane exposure, and inhibition of pathways associated with mitochondria-related apoptosis[15]. In a similar vein, we propose that the enhancement of mitochondrial-related apoptosis observed in LPS-stimulated nerve cells mediated by AT-17 contributes to its anesthetic efficacy. This improvement stems from AT-17's ability to rectify mitochondrial dysfunction within LPS-stimulated nerve cells. Key mechanisms identified include the inactivation of pathways leading to mitochondrial apoptosis, suppression of CYTC release into the cytoplasm, and enhancement of both mitochondrial morphology and MMP, thereby culminating in a reduction in neuronal apoptotic events triggered by LPS stimulation. Furthermore, this study marks the first exploration into the relationship between mitochondrial-related apoptosis and the anesthetic function of LA under inflammatory conditions.

Abnormal neuronal apoptosis has been observed in models of neuropathic pain and inflammatory pain, which is closely associated with the pain response in rats. Our study demonstrated that AT-17 treatment in an inflammatory model of mandibular tooth extraction could reduce apoptosis of the inferior alveolar nerve tissue. Additionally, ABT-737, a mitochondrial apoptosis activator, was found to exacerbate the analgesic effects of AT-17 on both short-term and long-term pain responses in rats. This finding highlights the significance of mitochondrial-related apoptosis in mediating the therapeutic role of AT-17 under inflammatory conditions.

In a similar vein, Hu et al. reported increased neuronal apoptosis on Days 3 and 7 following nerve injury in a chronic contraction injury (CCI) rat model[16]. Fan et al. further established that injecting CFA into the hind paw of rats not only intensified neuronal apoptosis but also elevated the expression levels of Bax and CASPASE-3 within neurons[17]. Moreover, inhibiting neuronal apoptosis has been shown to alleviate pain behavior in both experimental models. However, our findings indicated that treatment with AT-17 for just 1 h did not elevate levels of neuronal apoptosis, suggesting that its short-term analgesic effects are unlikely to be linked to nerve cell death. This observation may be attributed to insufficient induction of neuronal apoptosis by local LPS injection within this brief timeframe, resulting in no detectable effect from AT-17. Nevertheless, pre-inducing neuronal apoptosis with ABT-737 aggravated both neuron cell death and inhibited short-term analgesic outcomes associated with AT-17; this suggested a close relationship between the effects exerted by AT-17 and mitochondrial-related neuronal apoptosis.

Our previous findings indicated that mtROS generation played a critical role in the anti-inflammatory effects of AT-17. Given the central function of mtROS in mitochondrial activity, dysregulated mtROS production can lead to oxidative stress, mitochondrial dysfunction, and apoptosis through mechanisms involving oxidative damage and activation of mitochondrial permeability transition pores[18]. What's more, the production of mtROS and the degree of inflammation in nerve cells can interact with each other, forming a vicious cycle[19]. Our results demonstrated that T-BHP can negate the protective effect of AT-17 on LPS-stimulated neuronal cells; conversely, MT exhibited synergistic properties by enhancing the protective effects of AT-17. This highlighted the significance of mtROS in modulating mitochondrial-related neuronal responses to AT-17. Similarly, Li et al.[20] discovered that treatment with T-BHP elevated ROS levels in PC12 cells, which subsequently induced neuronal mitochondrial dysfunction and increased expression levels of autophagy-specific markers LC3 and SQSTM1/P62, ultimately contributing to neurotoxicity. In an *in vitro* model for Parkinson's disease, Yu et al.[21] reported that pretreatment with MT markedly diminished mtROS production in nerve cells while increasing expression levels of autophagy-related genes such as *ATG5* and *LC3II*; concurrently, it decreased P62 expression and activated CASPASE3, thereby reducing neuronal apoptosis associated with Parkinson's disease. Furthermore, bupivacaine has been shown to induce mtROS generation alongside decreased MMP, resulting in oxidative damage and cell apoptosis in both *in vitro* and *in vivo* studies involving neural cells. However, MT has demonstrated protective properties against this oxidative injury by mitigating cell apoptosis, effectively diminishing bupivacaine-induced neurotoxicity[22]. Additionally, it was found that MT pretreatment could block cocaine's provocative role on promoting mitochondrial autophagy while inducing cellular dysfunction through microglial activation, leading to neuroinflammation[23].

Activation of the NRF2 pathway serves as one of the primary defense mechanisms in response to ROS stimulation or other conditions associated with oxidative stress. The degradation of NRF2 mediated by KEAP1 diminishes, resulting in an accumulation of NRF2 within the nucleus where it binds to antioxidant response elements. This binding initiates the transcription of downstream antioxidant genes, including *NQO1*, *HO1*, glutathione synthase, glutathione reductase, and superoxide dismutase[24]. We found that AT-17 could activate the NRF2 pathway by inhibiting mtROS generation. Furthermore, TBHQ was observed to reverse the inhibitory effect of T-BHP on AT-17's ability to alleviate mitochondrial dysfunction and apoptosis in LPS-stimulated nerve cells. These findings suggested that the NRF2

signaling pathway played a significant role in mediating the neuroprotective effects of AT-17. In alignment with our results, several studies have demonstrated that the NRF2 pathway is implicated in various roles associated with lidocaine. For instance, Xue et al.[25] reported that SH-SY5Y cells exhibited concentration-dependent cytotoxicity following exposure to lidocaine; this was accompanied by elevated ROS levels and decreased nuclear expression of NRF2 protein along with increased cytoplasmic levels of NRF2. The activation of NRF2 has been shown to enhance the expressions of downstream antioxidant proteins and mitigate lidocaine-induced neurotoxicity. Moreover, after vascular endothelial cells were subjected to high glucose treatment, ropivacaine resulted in upregulated expressions of both NRF2 and HO1, thereby alleviating high glucose-induced ROS production and oxidative stress while providing a protective effect[26].

How did AT-17 inhibit mtROS production in nerve cells following LPS stimulation? It is well established that Na^+, the primary mechanism by which LA exerts its effects, can also function as a second messenger to regulate oxidative phosphorylation and redox signaling, thereby controlling mtROS production. Pablo Hernansanz-Agustín et al.[11] discovered that during acute hypoxia, the conformation of ETC complex I undergoes a transformation that drives mitochondrial matrix acidification and facilitates the release of free Ca^{2+} from calcium phosphate precipitation. In conjunction with NCLX activation, this process promotes the influx of cytoplasmic Na^+ into the mitochondrial matrix. Mitochondrial Na^+ then interacts with phospholipids, resulting in decreased mitochondrial membrane fluidity and reduced migration rates of free ubiquinone between complexes II and III, thus enhancing mtROS production at complex III. Additionally, Corte-Real BF et al. found that a high salt diet elevated intracellular Na^+ concentration, leading to increased entry of Na^+ into mitochondria *via* NCLX. This influx directly inhibited mitochondrial respiration at ETC complexes II/III, promoted mtROS generation, disrupted Treg mitochondrial functions, and induced metabolic reprogramming within these cells. Importantly, the detrimental effects of high salt on Treg dysfunction could be reversed through NCLX inhibition or blockade of mitochondrial Na^+ influx[27]. Our findings suggested that AT-17 may decrease both intracellular and mitochondrial Na^+ concentrations *via* NCLX channels, thereby restoring activities at ETC complexes I and III while inhibiting mtROS production.

There is limited research concerning mitochondrial-related apoptosis and the anesthetic properties of LAs. However, the relationship between mitochondria and Na_V, which are the primary targets of local anesthetic action, has been investigated. The anatomical structure demonstrating the co-localization of Na_V and mitochondria in the optic nerve suggests a close association between these two entities[28]. Additionally, an anatomical hub known as a couplon—formed by clusters of sodium channels in conjunction with mitochondria—has also been observed in cardiac myocytes[29]. Moreover, mtROS have been shown to be associated with the activity of cardiac Na_V. Research indicates that applying MT to inhibit mtROS generation can block the inhibitory effect of NADH on cardiac Na_V and reduce cardiac sodium current[30]. We proposed that the application of ABT-737 may obstruct the inhibitory function of AT-17 on Na_V in LPS-stimulated nerve cells, while MT treatment could reverse ABT-737's effects. This finding underscored the significant roles played by mitochondrial-related apoptosis and mtROS in mediating the anesthetic effect of AT-17 within an inflammatory context.

5. Conclusions

Herein, the novel oral LA AT-17 was demonstrated to play effective roles not only in chronic inflammation but also in acute inflammation, particularly in cases of oral acute inflammation. Furthermore, nerve cell apoptosis was found to be a significant factor in the inflammatory response associated with AT-17. Specifically, AT-17 can attenuate the production of mtROS in neural cells *via* the Na^+/NCLX/ETC signaling axis. The reduction of mtROS subsequently contributes to the activation of the NRF2 pathway and amelioration of LPS-induced mitochondrial dysfunction, ultimately resulting in decreased nerve cell apoptosis. Additionally, improvements related to mitochondrial apoptosis were linked to the inhibitory effects of AT-17 on voltage-gated sodium channels. Overall, our study represents the first development of a novel local anesthetic with effective analgesic properties within inflammatory environments; this could significantly enhance patient comfort during inflammatory procedures. To our knowledge, this is also the first instance elucidating the relationship between mitochondria-related apoptosis and anesthetic efficacy in local anesthetics, thus providing new insights for future drug development endeavors.

Acknowledgments

This study was supported by the National Natural Science Foundation of China (82425054 and 82273784); the Research and Develop Program, West China Hospital of Stomatology Sichuan University (RD-03-202004, China); Health Commission of Sichuan Province Medical Science and Technology Program(No. 24CGZH05, China); the 1.3.5 Projects for Disciplines of Excellence, West China Hospital, Sichuan University (ZYGD25002 and ZYGD23025, China); the Sichuan Science and Technology Programs (2024NSFSC0048, 2023ZYD0168, 2024YFFK0374 and 2023ZYD0168, China). The authors gratefully acknowledge the National Natural Science Foundation of China (82425054 and 82273784), the 1.3.5 Project for Disciplines of Excellence, West China Hospital, Sichuan University (ZYGD25002 and ZYGD23025, China), Nature Science Foundation of Sichuan Province (2024NSFSC0048, China), and Sichuan Science and Technology Program (2023ZYD0168, China).

Author contributions

Conceptualization: Ling Ye, Jin Liu, Xinhua Liang, Bowen Ke; Designed and performed research: Yihang Hao, Wenrui Gai, Wencheng Liu; Assisted in the experiments: Rongjia Shi, Yongzhen Tan, Ting Kang, Ao Hai, Yi Zhao, Yaling Tang; Data analysis: Haofan Wang, Wencheng Liu, Shilong Hu, Ma Bo; Manuscript writing, review and editing: Haofan Wang, Yihang Hao, Wenrui Gai, Xinhua Liang, Bowen Ke. All authors critically reviewed and approved the manuscript.

Conflicts of interest

The authors declare no conflicts of interest.

Appendix A. Supporting Information

Supporting information to this article can be found online at https://doi.org/10.1016/j.apsb.2025.09.001.

References

1. Nivedha V, Sherwood IA, Abbott PV, Ramaprabha B, Bhargavi PV. Pre-operative ketorolac efficacy with different anesthetics, irrigants during single visit root canal treatment of mandibular molars with acute irreversible pulpitis. *Aust Endod J* 2020;**46**:343−50.
2. Akural E, Jarvimaki V, Alaniska K, Oikarinen K, Alahuhta S. Peripheral morphine reduces acute pain in inflamed tissue after third molar extraction: a double-blind, randomized, active-controlled clinical trial. *Scand J Pain* 2016;**11**:59−64.
3. Brenner D, Mak TW. Mitochondrial cell death effectors. *Curr Opin Cell Biol* 2009;**21**:871−7.
4. Hao Y, Wang H, Liu X, Gai W, Hu S, Liu W, et al. Deep simulated annealing for the discovery of novel dental anesthetics with local anesthesia and anti-inflammatory properties. *Acta Pharm Sin B* 2024; **14**:3086−109.
5. Martinez-Garcia MA, Miguelanez-Medran BC, Goicoechea C. Animal models in the study and treatment of orofacial pain. *J Clin Exp Dent* 2019;**11**:e382−90.
6. Maltos KL, Menezes GB, Caliari MV, Rocha OA, Santos JM, Alves DL, et al. Vascular and cellular responses to pro-inflammatory stimuli in rat dental pulp. *Arch Oral Biol* 2004;**49**:443−50.
7. Zhang H, Li N, Li Z, Li Y, Yu Y, Zhang L. The involvement of caspases in neuroinflammation and neuronal apoptosis in chronic pain and potential therapeutic targets. *Front Pharmacol* 2022;**13**:898574.
8. Liao MF, Lu KT, Hsu JL, Lee CH, Cheng MY, Ro LS. The role of autophagy and apoptosis in neuropathic pain formation. *Int J Mol Sci* 2022;**23**:2685.
9. Bock FJ, Tait SWG. Mitochondria as multifaceted regulators of cell death. *Nat Rev Mol Cell Biol* 2020;**21**:85−100.
10. Tong T, Qin X, Jiang Y, Guo H, Wang X, Li Y, et al. A novel CREB5/TOP1MT axis confers cisplatin resistance through inhibiting mitochondrial apoptosis in head and neck squamous cell carcinoma. *BMC Med* 2022;**20**:231.
11. Hernansanz-Agustin P, Choya-Foces C, Carregal-Romero S, Ramos E, Oliva T, Villa-Pina T, et al. Na^+ controls hypoxic signalling by the mitochondrial respiratory chain. *Nature* 2020;**586**:287−91.
12. Johnson ME, Uhl CB, Spittler KH, Wang H, Gores GJ. Mitochondrial injury and caspase activation by the local anesthetic lidocaine. *Anesthesiology* 2004;**101**:1184−94.
13. Nouette-Gaulain K, Dadure C, Morau D, Pertuiset C, Galbes O, Hayot M, et al. Age-dependent bupivacaine-induced muscle toxicity during continuous peripheral nerve block in rats. *Anesthesiology* 2009; **111**:1120−7.
14. Chen Z, Jin Z, Xia Y, Zhao S, Xu X, Papadimos TJ, et al. The protective effect of lipid emulsion in preventing bupivacaine-induced mitochondrial injury and apoptosis of H9C2 cardiomyocytes. *Drug Deliv* 2017;**24**:430−6.
15. Li J, Zhu X, Yang S, Xu H, Guo M, Yao Y, et al. Lidocaine attenuates cognitive impairment after isoflurane anesthesia by reducing mitochondrial damage. *Neurochem Res* 2019;**44**:1703−14.
16. Hu Q, Fang L, Li F, Thomas S, Yang Z. Hyperbaric oxygenation treatment alleviates CCI-induced neuropathic pain and decreases spinal apoptosis. *Eur J Pain* 2015;**19**:920−8.
17. Fan YF, Guan SY, Luo L, Li YJ, Yang L, Zhou XX, et al. Tetrahydroxystilbene glucoside relieves the chronic inflammatory pain by inhibiting neuronal apoptosis, microglia activation, and GluN2B overexpression in anterior cingulate cortex. *Mol Pain* 2018;**14**: 1744806918814367.
18. Peoples JN, Saraf A, Ghazal N, Pham TT, Kwong JQ. Mitochondrial dysfunction and oxidative stress in heart disease. *Exp Mol Med* 2019; **51**:1−13.
19. Zhou X, Wang J, Yu L, Qiao G, Qin D, Yuen-Kwan Law B, et al. Mitophagy and cGAS−STING crosstalk in neuroinflammation. *Acta Pharm Sin B* 2024;**14**:3327−61.
20. Li Z, Jiang T, Lu Q, Xu K, He J, Xie L, et al. Berberine attenuated the cytotoxicity induced by t-BHP *via* inhibiting oxidative stress and mitochondria dysfunction in PC-12 cells. *Cell Mol Neurobiol* 2020;**40**: 587−602.
21. Yu Q, Zhang R, Li T, Yang L, Zhou Z, Hou L, et al. Mitochondrial hydrogen peroxide activates PTEN and inactivates Akt leading to autophagy inhibition-dependent cell death in neuronal models of parkinson's disease. *Mol Neurobiol* 2023;**60**:3345−64.
22. Liu ZJ, Xu SY, Ji ZH, Xu HL, Zhao W, Xia ZY, et al. Mechanistic study of mtROS−JNK−SOD2 signaling in bupivacaine-induced neuron oxidative stress. *Aging (Albany NY)* 2020;**12**:13463−76.
23. Thangaraj A, Periyasamy P, Guo ML, Chivero ET, Callen S, Buch S. Mitigation of cocaine-mediated mitochondrial damage, defective mitophagy and microglial activation by superoxide dismutase mimetics. *Autophagy* 2020;**16**:289−312.
24. He F, Ru XL, Wen T. NRF2, a transcription factor for stress response and beyond. *Int J Mol Sci* 2020;**21**:4777.
25. Xue Y, Wang AZ. DJ-1 plays a neuroprotective role in SH-SY5Y cells by modulating Nrf2 signaling in response to lidocaine-mediated oxidative stress and apoptosis. *Kaohsiung J Med Sci* 2020;**36**:630−9.
26. Lv H, Cheng Q, Li Y, Zhang Y, Chen JW, Chen W. The protective effects of ropivacaine against high glucose-induced brain microvascular endothelial injury by reducing MMPs and alleviating oxidative stress. *Neurotox Res* 2021;**39**:851−9.
27. Corte-Real BF, Hamad I, Arroyo Hornero R, Geisberger S, Roels J, Van Zeebroeck L, et al. Sodium perturbs mitochondrial respiration and induces dysfunctional Tregs. *Cell Metab* 2023;**35**:299−315.e8.
28. Boiteux C, Vorobyov I, French RJ, French C, Yarov-Yarovoy V, Allen TW. Local anesthetic and antiepileptic drug access and binding to a bacterial voltage-gated sodium channel. *Proc Natl Acad Sci U S A* 2014;**111**:13057−62.
29. Perez-Hernandez M, Leo-Macias A, Keegan S, Jouni M, Kim JC, Agullo-Pascual E, et al. Structural and functional characterization of a $Na_v1.5$-mitochondrial couplon. *Circ Res* 2021;**128**:419−32.
30. Liu M, Liu H, Dudley Jr SC. Reactive oxygen species originating from mitochondria regulate the cardiac sodium channel. *Circ Res* 2010;**107**: 967−74.